J|A|C|S
ARTICLES
Published on Web 08/23/2002

Long-Range Magnetization Transfer between Uncoupled Nuclei by Dipole−Dipole Cross-Correlated Relaxation: A Precise Probe of β-Sheet Geometry in Proteins

Jerome Boisbouvier and Ad Bax*

Contribution from the Laboratory of Chemical Physics, National Institutes of Diabetes and Digestive and Kidney Diseases, National Institutes of Health, Bethesda, Maryland 20892-0520

Received April 9, 2002

Abstract: Interference between dipolar interactions in covalently linked $^{13}C-^{1}H$ and nonlinked $^{1}H-^{1}H$ pairs can be used to generate antiphase magnetization between noncoupled spins. The buildup rate of such antiphase terms is highly sensitive to local geometry, in particular the interproton distance and the $^{13}C-^{1}H-^{1}H$ internuclear angle. These rates have been measured for opposing $C_\alpha H_\alpha$ pairs in antiparallel β-sheets in the third Igg-binding domain of protein G (GB3) and in HIV protease, complexed with the inhibitor DMP323. For GB3, good agreement with the 1.1-Å crystal structure is found. However, this agreement rapidly deteriorates with decreasing resolution of the corresponding X-ray structure. For HIV protease, two separate crystal structures that differ by less than 0.2 Å from one another exhibit lower agreement in their predicted cross-correlated relaxation rates relative to one another than is found between experimental rates and the average of the rates predicted for the two structures. These data indicate that quantitative measurement of these cross-correlated relaxation rates can provide highly accurate structural information in macromolecules.

NMR has become a well-established method for determining the three-dimensional structure of proteins and nucleic acids. Most such structural studies have been based primarily on interproton distances, determined from $^{1}H-^{1}H$ NOEs, and torsion angles, derived from J couplings.[1] More recently, a host of other structural parameters have been introduced, including the measurement of internuclear vector orientations from dipolar couplings in partly oriented systems, and relative internuclear vector orientations from cross-correlated relaxation.[2]

Cross-correlated relaxation relies on the interference between two separate relaxation mechanisms, which leads to nonexponential relaxation in a manner that is a function of the relative orientations of the magnetic interactions underlying these relaxation mechanisms.[3−7] Besides providing structural information, in cases of known geometry, interference effects between covalently linked spins also can yield information on the CSA tensor, which is related to local conformation and hydrogen bonding.[8−11]

Although it has been well recognized that, at least in principle, measurement of cross-correlated relaxation is applicable to any two pairs of interactions in a macromolecule, irrespective of their relative distance,[2] in practice most work has focused on pairs of spins connected by a short J-coupling network that permits efficient generation of multispin coherences. Measurement of cross-correlated double-quantum and zero-quantum relaxation rates has been used to measure torsion angles in proteins[2,12−18] and in nucleic acids[19,20] and recently also has been used to obtain structural information on spins connected by J coupling through hydrogen bonds.[21−23]

A different set of experiments is based on cross-correlated relaxation between a local interaction and the dipolar interaction with the magnetic-field-dependent net magnetization of a fast relaxing electron of a paramagnetic site in the protein.[24,25] Owing

* Address correspondence to this author. E-mail: bax@nih.gov.

(1) Wüthrich, K. *NMR of Proteins and Nucleic Acids*; John Wiley & Sons: New York, 1986.
(2) Reif, B.; Hennig, M.; Griesinger, C. *Science* **1997**, *276*, 1230−1233.
(3) Werbelow, L. G.; Grant, D. M. *Adv. Magn. Reson.* **1977**, *9*, 189−299.
(4) Vold, R. L.; Vold, R. R. *Prog. Nucl. Magn. Reson. Spectrosc.* **1978**, *12*, 79−133.
(5) Goldman, M. *J. Magn. Reson.* **1984**, *60*, 437−452.
(6) Brutscher, B. *Concepts Magn. Reson.* **2000**, *12*, 207−229.
(7) Kumar, A.; Grace, R. C. R.; Madhu, P. K. *Prog. Nucl. Magn. Reson. Spectrosc.* **2000**, *37*, 191−319.
(8) Tjandra, N.; Bax, A. *J. Am. Chem. Soc.* **1997**, *119*, 9576−9577.
(9) Tessari, M.; Vis, H.; Boelens, R.; Kaptein, R.; Vuister, G. W. *J. Am. Chem. Soc.* **1997**, *119*, 8985−8990.
(10) Tjandra, N.; Bax, A. *J. Am. Chem. Soc.* **1997**, *119*, 8076−8082.
(11) Boisbouvier, J.; Brutscher, B.; Pardi, A.; Marion, D.; Simorre, J. P. *J. Am. Chem. Soc.* **2000**, *122*, 6779−6780.
(12) Yang, D. W.; Konrat, R.; Kay, L. E. *J. Am. Chem. Soc.* **1997**, *119*, 11938−11940.
(13) Pelupessy, P.; Chiarparin, E.; Ghose, R.; Bodenhausen, G. *J. Biomol. NMR* **1999**, *13*, 375−380.
(14) Chiarparin, E.; Pelupessy, P.; Ghose, R.; Bodenhausen, G. *J. Am. Chem. Soc.* **1999**, *121*, 6876−6883.
(15) Pelupessy, P.; Chiarparin, E.; Ghose, R.; Bodenhausen, G. *J. Biomol. NMR* **1999**, *14*, 277−280.
(16) Chiarparin, E.; Pelupessy, P.; Ghose, R.; Bodenhausen, G. *J. Am. Chem. Soc.* **2000**, *122*, 1758−1761.
(17) Kloiber, K.; Konrat, R. *J. Am. Chem. Soc.* **2000**, *122*, 12033−12034.
(18) Kloiber, K.; Schüler, W.; Konrat, W. *J. Biomol. NMR* **2002**, *22*, 349−363.
(19) Felli, I. C.; Richter, C.; Griesinger, C.; Schwalbe, H. *J. Am. Chem. Soc.* **1999**, *121*, 1956−1957.
(20) Richter, C.; Reif, B.; Griesinger, C.; Schwalbe, H. *J. Am. Chem. Soc.* **2000**, *122*, 12728−12781.
(21) Skrynnikov, N. R.; Konrat, R.; Muhandiram, D. R.; Kay, L. E. *J. Am. Chem. Soc.* **2000**, *122*, 7059−7071.
(22) Chiarparin, E.; Rudisser, S.; Bodenhausen, G. *ChemPhysChem* **2001**, *2*, 41−45.
(23) Riek, R. *J. Magn. Reson.* **2001**, *149*, 149−153.

to the large dipole moment of such Curie spin magnetization, relaxation interference effects can be observed up to substantial distances away from the paramagnetic site,[26,27] in addition to exploiting the direct paramagnetic effects such as pseudo-contact shifts and relaxation enhancement for structural purposes.[28−31]

The present study relies on a different type of cross-correlated relaxation measurement in proteins: the transfer of magnetization between hydrogens that are not connected by a *J*-coupling network. The possibility of transferring net magnetization from one spin to another through relaxation interference has long been recognized,[32−35] and several applications to magnetization transfer have been described.[33,36] For example, Wimperis and Bodenhausen demonstrated that, in a nearly linear arrangement of four protons, A, B, C, and D, magnetization transfer between B and C could be generated in the absence of B−C scalar coupling.[33] Here, we focus on relaxation interference between the $C_\alpha{}^1-H_\alpha{}^1$, $H_\alpha{}^1-H_\alpha{}^2$ and $H_\alpha{}^2-C_\alpha{}^2$ dipolar interactions in opposing $^{13}C_\alpha-^1H_\alpha$ groups in β-sheets. We demonstrate that net magnetization transfer is readily possible and contains information that is very sensitive to the relative position of such groups. Relaxation interference effects depend primarily on zero-frequency spectral density terms, causing cross-correlated relaxation rates to increase with molecular size. Application of these new techniques is therefore not restricted to small systems.

Materials and Methods

All NMR experiments were carried out on Bruker DRX spectrometers, operating at 600-MHz ^1H frequency. For all experiments, the ^1H carrier was positioned on the HOD resonance and the ^{13}C carrier at 43 ppm. All data were processed and analyzed with NMRPipe.[37] Data apodization utilized a 90°-shifted squared sine-bell function in the directly detected dimension and a sine-bell function shifted by 90° in the indirect dimension. Data were zero-filled by at least a factor of 2 in all dimensions prior to Fourier transformation.

Two different samples were used in the present study. The first sample contained 1.8 mM ^{13}C,^{15}N-labeled third Igg-binding domain from streptococcal protein G (further referred to as GB3) dissolved in D_2O, pH 5.6, 50 mM sodium phosphate. For unidirectional transfer schemes, data were recorded at 15 °C on a spectrometer equipped with a triple-resonance, three-axes pulsed field gradient probehead, optimized for ^1H detection. For the "out-and-back" experiments, the sample temperature was set to 6.5 °C, and the spectrometer used was equipped with a cryogenic, triple-resonance probehead equipped with a *z*-axis pulsed field gradient. A second sample contained 0.4 mM (dimer) ^{13}C,^{15}N-labeled HIV-1 protease complexed with unlabeled DMP323 inhibitor, dissolved in D_2O, pH 5.6, 25 mM sodium phosphate.[38,39] Data were acquired at 27 °C using a cryogenic probehead with a triple-resonance, *z*-axis pulsed field gradient probehead, optimized for ^1H detection.

Theoretical Basis

Here, we consider the case of an isolated system of three spins, *A*, *M*, and *X*, each with negligible CSA. The master equation describing the spin dynamics has a block-diagonal matrix representation, where the evolution of the four *M*-spin single-quantum coherences is described by[40]

$$\frac{d}{dt}\begin{pmatrix} M_+(t) \\ 2M_+A_z(t) \\ 2M_+X_z(t) \\ 4M_+A_zX_z(t) \end{pmatrix} = -(L + iK)\begin{pmatrix} M_+(t) \\ 2M_+A_z(t) \\ 2M_+X_z(t) \\ 4M_+A_zX_z(t) \end{pmatrix} \quad (1)$$

with

$$L = \begin{pmatrix} R(M_+) & 0 & 0 & \Gamma^{DD,DD}_{MA,MX} \\ 0 & R(2M_+A_z) & \Gamma^{DD,DD}_{MA,MX} & 0 \\ 0 & \Gamma^{DD,DD}_{MA,MX} & R(2M_+X_z) & 0 \\ \Gamma^{DD,DD}_{MA,MX} & 0 & 0 & R(4M_+A_zX_z) \end{pmatrix}$$

$$K = \begin{pmatrix} \omega_M & \pi J_{MA} & \pi J_{MX} & 0 \\ \pi J_{MA} & \omega_M & 0 & \pi J_{MX} \\ \pi J_{MX} & 0 & \omega_M & \pi J_{MA} \\ 0 & \pi J_{MX} & \pi J_{MA} & \omega_M \end{pmatrix}$$

where ω_M is the Larmor frequency of spin *M*, J_{IS} the scalar coupling between spins *I* and *S*, $R(I)$ is the autorelaxation rate of coherence *I*, and $\Gamma^{DD,DD}_{MA,MX}$ represents the dipole−dipole cross-correlation rates between spin vectors *MA* and *MX*. Equation 1 describes how *M*-spin in-phase magnetization can be transferred to two-spin antiphase coherence, either by scalar coupling or by cross-correlated relaxation.[32] Neglecting internal dynamics, the relaxation rates for a spherical macromolecule in the slow tumbling limit, are given by[7]

$$R(2M_+A_z) \approx R(2M_+X_z) \approx R(4M_+A_zX_z) \approx R(M_+) \approx R_2 \quad (2)$$

$$\Gamma^{DD,DD}_{MA,MX} \approx \frac{\tau_c}{5}\xi^{DD}_{MA}\,\xi^{DD}_{MX}(3\cos^2\theta - 1) \quad (3)$$

where θ is the angle between vectors *MA* and *MX*, $\xi^{DD}_{IS} = -(\mu_o\hbar\gamma_I\gamma_S)/(4\pi\langle r^3_{IS}\rangle)$, and r_{IS} the distance between nuclei *I* and *S*. In the case of anisotropic rotational diffusion, the correlation time τ_c needs to be replaced by the corresponding spectral density functions.[41−43] Due to its geometrical dependence, the dipole−dipole cross-correlation rate is maximum for a linear alignment of the three spins, with *M* occupying the central position. For the $^{13}C-^1H-^1H$ spin system considered below, $J_{MX} = 0$. For such an isolated three-spin system, the resulting violation of the secular approximation introduces only spectral density terms at $J(\omega_H)$, which are negligible in the slow tumbling

(24) Bertini, I.; Luchinat, C.; Tarchi, D. *Chem. Phys. Lett.* **1993**, *203*, 445−449.
(25) Qin, J.; Delaglio, F.; Lamar, G. N.; Bax, A. *J. Magn. Reson. Ser. B* **1993**, *102*, 332−336.
(26) Ghose, R.; Prestegard, J. H. *J. Magn. Reson.* **1997**, *128*, 138−143.
(27) Boisbouvier, J.; Gans, P.; Blackledge, M.; Brutscher, B.; Marion, D. *J. Am. Chem. Soc.* **1999**, *121*, 7700−7701.
(28) Bertini, I.; Luchinat, C. *NMR of paramagnetic molecules in biological systems*; Benjamin/Cummings: Menlo Park, 1986.
(29) Gochin, M.; Roder, H. *Protein Sci.* **1995**, *4*, 296−305.
(30) Banci, L.; Bertini, I.; Savellini, G. G.; Romagnoli, A.; Turano, P.; Cremonini, M. A.; Luchinat, C.; Gray, H. B. *Proteins−Struct., Funct. Genet.* **1997**, *29*, 68−76.
(31) Hus, J. C.; Marion, D.; Blackledge, M. *J. Mol. Biol.* **2000**, *298*, 927−936.
(32) Wimperis, S.; Bodenhausen, G. *Chem. Phys. Lett.* **1987**, *140*, 41−45.
(33) Wimperis, S.; Bodenhausen, G. *Mol. Phys.* **1989**, *66*, 897−919.
(34) Dalvit, C. *J. Magn. Reson.* **1992**, *97*, 645−650.
(35) Bruschweiler, R.; Ernst, R. R. *J. Chem. Phys.* **1992**, *96*, 1758−1766.
(36) Vincent, S. J. F.; Zwahlen, C. *J. Am. Chem. Soc.* **2000**, *122*, 8307−8308.
(37) Delaglio, F.; Grzesiek, S.; Vuister, G. W.; Zhu, G.; Pfeifer, J.; Bax, A. *J. Biomol. NMR* **1995**, *6*, 277−293.
(38) Louis, J. M.; Clore, G. M.; Gronenborn, A. M. *Nat. Struct. Biol.* **1999**, *6*, 868−875.
(39) Ishima, R.; Louis, J. M.; Torchia, D. A. *J. Biomol. NMR* **2001**, *21*, 167−171.
(40) Redfield, A. G. *Adv. Magn. Reson.* **1965**, *1*, 1−32.
(41) Spiess, H. W. *NMR: Basic Princ. Prog.* **1978**, *15*, 55−214.
(42) Chung, J.; Oldfield, E.; Thevand, A.; Werbelow, L. *J. Magn. Reson.* **1992**, *100*, 69−81.
(43) Cuperlovic, M.; Palke, W. E.; Gerig, J. T.; Gray, G. A. *J. Magn. Reson. Ser. B* **1996**, *110*, 26−38.

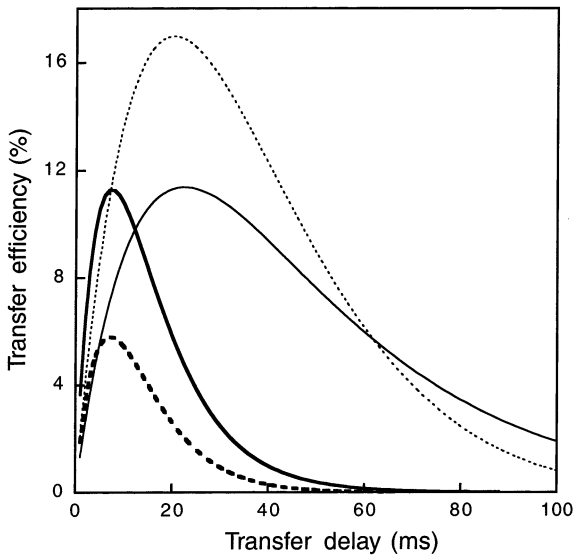

Figure 1. Comparison of the calculated transfer efficiency mediated through dipole−dipole cross-correlated relaxation (solid lines) and through scalar coupling (dashed lines) as a function of the transfer delay. The curves correspond to $H_x^1 \rightarrow 4H_x^1C_z^1H_z^2$ conversion in a $\{C^1,H^1,H^2\}$ spin system with the standard geometry found in an antiparallel β-sheet ($r_{H1H2} = 2.4$ Å and $\theta_1 = 25°$, see Figure 2 for notation), or $H_x^1 \rightarrow 2H_y^1H_z^2$ for J_{H1H2}-mediated transfer with $J_{H1H2} = 7$ Hz. The effects of protein protons other than H^1 or H^2 have been accounted for by adding to the transverse autorelaxation rates an additional $^1H-^1H$ dipolar contribution corresponding to a 2-Å distance. Thin lines correspond to $\tau_c = 6$ ns ($R_2 = 46$ Hz and $\Gamma^{DD,DD}_{C1H1,H1H2} = 14$ Hz), and bold lines correspond to $\tau_c = 18$ ns ($R_2 = 139$ Hz and $\Gamma^{DD,DD}_{C1H1,H1H2} = 42$ Hz).

limit. The effect of the invalidity of the secular approximation in a larger spin system, such as that found in proteins, is discussed in the section, Correlation with Structure (below).

With the initial condition $4M_+A_zX_z(0) = 0$ and $M_+(0) = 1$, in the absence of scalar coupling evolution, one obtains

$$\begin{cases} M_+(t) = \cosh(-\Gamma^{DD,DD}_{MA,MX}t)\exp(-R_2t) \\ 4M_+A_zX_z(t) = \sinh(-\Gamma^{DD,DD}_{MA,MX}t)\exp(-R_2t) \end{cases} \quad (4)$$

Similarly, with initial conditions $2M_+A_z(0) = 0$ and $2M_+X_z(0) = 1$, the solution for cross-correlation mediated transfer is

$$\begin{cases} 2M_+X_z(t) = \cosh(-\Gamma^{DD,DD}_{MA,MX}t)\exp(-R_2t) \\ 2M_+A_z(t) = \sinh(-\Gamma^{DD,DD}_{MA,MX}t)\exp(-R_2t) \end{cases} \quad (5)$$

Due to the symmetry of eq 1, interchanging the initial condition for eqs 4 and 5 simply results in a permutation of the sinh and cosh terms.

As both the cross-relaxation and autorelaxation rates increase simultaneously with the rotational diffusion correlation time, the efficiency of cross-correlation mediated transfer does not depend on the molecular size, provided that the transfer delay is adjusted to its optimal value: $\tau_{opt} \approx (R_2)^{-1}$ (Figure 1). Hence, the cross-correlation mechanism is particularly useful for transferring magnetization between noncoupled or weakly coupled spins in large biomacromolecules, for which the transverse autorelaxation rate precludes efficient transfer through scalar couplings.

Results and Discussion

The feasibility of cross-correlated relaxation for generating net magnetization transfer between uncoupled spins in a protein

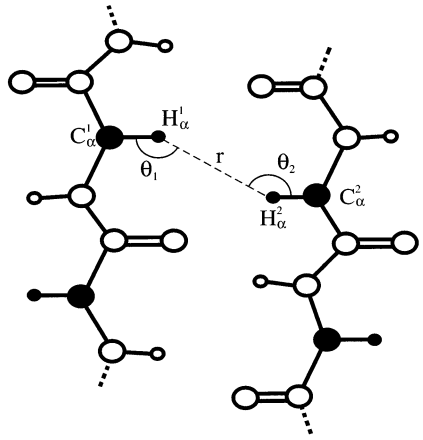

Figure 2. Definition of geometrical parameters involved in RACT in antiparallel β-sheet.

will be demonstrated for $\{^{13}C_\alpha{}^1,{}^1H_\alpha{}^1,{}^1H_\alpha{}^2\}$ spin systems, as found in antiparallel β-sheets. However, a range of other applications can also be envisioned. The relevant geometric parameters are illustrated in Figure 2. The close proximity typically found between opposing H_α spins in β-sheets and the relative orientation of the $^{13}C^1_\alpha-{}^1H^1_\alpha$, $^1H^1_\alpha-{}^1H^2_\alpha$, and $^{13}C^2_\alpha-{}^1H^2_\alpha$ vectors result in substantial cross-correlated relaxation rates, involving dipolar interaction of the $C^1_\alpha-H^1_\alpha$ (or $C^2_\alpha-H^2_\alpha$) pair and the dipolar interaction between the nonbonded $H^1_\alpha-H^2_\alpha$ pair. Below, these two dipole−dipole cross-correlated relaxation rates will be denoted $\Gamma_1 = \Gamma^{DD,DD}_{C1H1,H1H2}$ and $\Gamma_2 = \Gamma^{DD,DD}_{C2H2,H2H1}$.

As dipole−dipole cross-correlated transfer of magnetization involves up to four spins, the most general implementation of the method would be a four-dimensional scheme with each frequency dimension corresponding to one of the nuclei involved. In practice, it is more convenient to implement the experiments as 2D or 3D versions of such a 4D scheme, such that adequate digital resolution can be obtained within a limited total measuring time. As is the case for the regular triple-resonance NMR experiments, different transfer modes can be employed: unidirectional and "out-and-back". In the unidirectional experiments, magnetization originating on the first proton is transferred by the dipole−dipole cross-correlation mechanism (originally named RACT, for relaxation-allowed coherence transfer)[32] to antiphase magnetization on the second proton, which subsequently is rephased by a second RACT process, prior to detection of the second proton. The net transfer then depends on two separate RACT processes, each with its own geometric dependence. In the "out-and-back" mode, magnetization on the first proton is transferred by RACT to antiphase magnetization on the second proton, where it evolves for a variable amount of time, prior to transfer back to the first proton by the same RACT process. Quantitative analysis of the spectral intensities observed in the "out-and-back" version is therefore simpler as, besides the $H^1_\alpha-H^2_\alpha$ distance, it depends only on the angle θ_1 in Figure 2, whereas intensity in the unidirectional version is a function of both θ_1 and θ_2. Both modes of implementation are discussed below.

Unidirectional Transfer Schemes. Figure 3 shows 2D and 3D implementations of the unidirectional transfer. The 2D RACT pulse scheme employed here is very similar to a standard inverse heteronuclear two-dimensional HSQC experiment,[44] but with the last INEPT transfer replaced by a two-step RACT

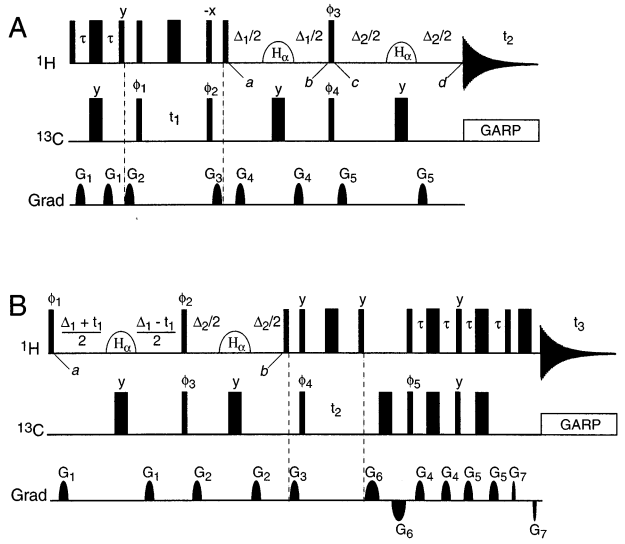

Figure 3. Pulse schemes for unidirectional RACT. (A) Two-dimensional $\{^{13}C\}-^{1}H \rightarrow {}^{1}H-\{^{13}C\}$ transfer scheme, where {} brackets mark the passive nuclei involved in cross-correlation, covalently linked to protons involved in the magnetization transfer. (B) Three-dimensional $\{^{13}C\}-^{1}H \rightarrow {}^{1}H-{}^{13}C$ transfer scheme. Narrow and wide pulses correspond to flip angles of 90° and 180°, respectively. Unless specified, pulses are applied along the *x*-axis. Shaped ^{1}H pulses are of the 180° REBURP type[58] (3.1-ms duration at 600 MHz, for a 2.1-ppm bandwidth inversion), centered on the HOD resonance. Their selective character suppresses $^{3}J_{HH}$ dephasing, which increases sensitivity, particularly if the condition $^{3}J_{H\alpha H\beta}\Delta_{1,2} \ll 1$ does not apply. During ^{13}C evolution, $^{13}C'$ is decoupled by application of a selective $^{13}C'$ 180° pulse and ^{15}N by GARP decoupling[59] (not shown). INEPT transfer delays, τ, are 1.63 ms. In (A), $\{\Delta_1,\Delta_2\}$ durations are set to $\{n/^{1}J_{CH},(m+0.5)/^{1}J_{CH}\}$, where *m* and *n* are integers. Δ_1 and Δ_2 values include the ^{1}H REBURP pulse duration, scaled by 0.9.[60] Quadrature detection in the ^{13}C dimension is achieved by incrementing ϕ_1 in the usual States-TPPI manner. Phase cycling: $\phi_1 = x,-x$; $\phi_2 = 2(x),2(-x)$; $\phi_3 = 8(x),8(-x)$; $\phi_4 = 4(y),4(-y)$; receiver = $x,-x,-x,x$. All gradients are sine-bell shaped, with a peak amplitude of 25 G/cm and durations of $G_{1,2,3,4,5} = 0.7$, 0.2, 0.3, 0.5, 0.6 ms. In (B), $\{\Delta_1,\Delta_2\}$ durations are $\{(m+0.5)/^{1}J_{CH},n/^{1}J_{CH}\}$. The relative length of gradients G_6 and G_7 is γ_H/γ_N, but this ratio is fine-adjusted to ensure optimal decoding. Quadrature detection in the ^{13}C dimension is achieved by incrementing ϕ_5 together with inverting the sign of G_6;[45] in the t_1 ^{1}H dimension, quadrature is achieved by phase incrementation of ϕ_1 in the usual States-TPPI manner. Phase cycling: $\phi_1 = y$; $\phi_2 = 2(x),2(-x)$; $\phi_3 = y,-y$; $\phi_4 = x,-x$; $\phi_5 = -x$; receiver = $x,-x$. All gradients are sine-bell shaped and applied in the *z* direction, with peak amplitudes of 25 G/cm and durations of $G_{1,2,3,4,5,6,7} = 0.2$, 0.1, 0.25, 0.14, 0.21, 1, 0.2515 ms.

scheme. At time point *a*, the antiphase magnetization is described by operator $2H_y^1C_z^1$, which is modulated in the t_1 dimension by the frequency of C^1. Between points *a* and *b*, evolution due to ^{1}H chemical shift and homonuclear couplings is refocused by the shaped pulse applied on H_α, and the value of Δ_1 is adjusted to $n/^{1}J_{HC}$, where *n* is an integer, to rephase the evolution due to the scalar coupling between H^1 and C^1. During Δ_1, net evolution of magnetization then results only from cross-relaxation and autorelaxation. As described in the Theoretical Basis section, transverse magnetization at point *b* is described by

$$\sigma_b = [2H_y^1C_z^1 \cosh(-\Gamma_1\Delta_1) + 2H_y^1H_z^2 \sinh(-\Gamma_1\Delta_1)] \exp[-R_2\Delta_1] \quad (6)$$

At point *b*, phase cycling of the ^{13}C $90_{\phi4}$ pulse is used to eliminate the cosh term, while $2H_y^1H_z^2$ is converted into $2H_z^1H_y^2$ by the ^{1}H $90_{\phi3}$ pulse. This last term evolves again under influence of cross-correlated relaxation between points *c* and *d*, converting $2H_z^1H_y^2$ into $2C_z^2H_y^2$. However, the value of Δ_2 is tuned to $(n + 0.5)/^{1}J_{HC}$, such that this term is converted into in-phase H_x^2 magnetization at time point *d*:

$$\sigma_d = \sinh(-\Gamma_1\Delta_1)[4H_x^2H_z^1C_z^2 \cosh(-\Gamma_2\Delta_2) + H_x^2 \sinh(-\Gamma_2\Delta_2)] \exp[-R_2(\Delta_1 + \Delta_2)] \quad (7)$$

^{13}C decoupling during t_2 data acquisition destroys the three-spin term in eq 7, and only the in-phase H_x^2 signal will be detected. Simultaneously to the $C^1 \rightarrow H^2$ transfer described above, a similar $C^2 \rightarrow H^1$ transfer results from Γ_2 evolution during Δ_1 and Γ_1 during Δ_2. Therefore, if the β-sheet geometry corresponds to sufficiently large dipole−dipole cross-correlation rates, two in-phase cross-peaks at frequencies $(\omega_{C1},\omega_{H2})$ and $(\omega_{C2},\omega_{H1})$ will be observed for each H_α pair.

For the 3D analogue of the unidirectional RACT scheme, it is advantageous to insert the cross-correlation steps at the start of the pulse scheme (Figure 3B). This permits a gradient-enhanced reverse INEPT back to ^{1}H to be used for transfer of both the *x* and *y* components of evolved ^{13}C magnetization, thereby optimizing sensitivity.[45] The Δ_1 cross-correlation delay is tuned to $(n + 0.5)/^{1}J_{HC}$, such that H_x^1 magnetization at time point *a*, which as a result of cross-correlation evolves into $4H_x^1C_z^1H_z^2$, rephases under the influence of $^{1}J_{CH}$ into $2H_y^1H_z^2$. Delay Δ_1 simultaneously serves as a constant-time evolution period for ^{1}H, and therefore does not require any additional delay duration relative to the 2D scheme. The $90°_{\phi2}$ ^{1}H pulse subsequently converts $2H_y^1H_z^2$ into $2H_z^1H_y^2$, which as a result of cross-correlation during the subsequent delay Δ_2 (adjusted to $m/^{1}J_{HC}$) evolves into $2C_z^2H_y^2$.

At the end of the two-step RACT, the observable detected signal has been transferred from H_x^1 (present at time point *a*) to the two-spin term $2H_y^2C_z^2$ at time point *b*. The magnitude of this term is given by

$$\sigma_b = 2H_y^2C_z^2[\sinh(-\Gamma_1\Delta_1) \sinh(-\Gamma_2\Delta_2) \times \exp[-R_2(\Delta_1 + \Delta_2)]] \quad (8)$$

To minimize relaxation losses during the subsequent ^{13}C t_2 evolution period, the term is converted to $2H_x^2C_y^2$ two-spin coherence, prior to conversion back to single-quantum ^{13}C coherence, phase-encoding by the G_6 gradients, and a Rance−Kay transfer back to ^{1}H.[45] The net result is that, for each pair of opposing H_α atoms in an antiparallel β-sheet, two in-phase cross-peaks at frequencies $(\omega_{H1},\omega_{C2},\omega_{H2})$ and $(\omega_{H2},\omega_{C1},\omega_{H1})$ will be observed.

Out-and-Back Transfer Scheme. As discussed above, intensities observed in the unidirectional transfer scheme depend on both the θ_1 and θ_2 angles, complicating quantitative analysis. However, an out-and-back RACT experiment can be used which depends on only a single angle, thereby facilitating the evaluation of the dependence of dipole−dipole cross-correlation rates on local geometry. This scheme (Figure 4) is quite similar to that of Figure 3B, but magnetization originating on proton H^1, and converted into $2H_y^1H_z^2$ (time point *b*) as a result of Γ_1 cross-correlation and J_{C1H1} rephasing during Δ_1, is again transferred

(44) Bodenhausen, G.; Ruben, D. J. *Chem. Phys. Lett.* **1980**, *69*, 185−189.

(45) Kay, L. E.; Keifer, P.; Saarinen, T. *J. Am. Chem. Soc.* **1992**, *114*, 10663−10665.

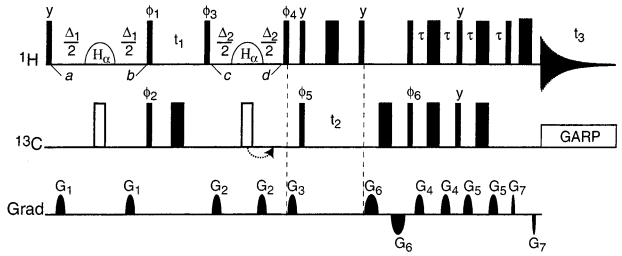

Figure 4. Pulse scheme for the 3D "out-and-back" RACT experiment, used for quantitative analysis. The open ^{13}C 180° pulses are applied at the indicated positions in the "out-and-back" RACT experiment; in the corresponding reference experiment the first open ^{13}C pulse is omitted, and the second one is shifted to 1.74 ms prior to the ^{1}H $90_{\phi 4}$ pulse. Phase cycling: $\phi_1 = 4(x),4(-x)$; $\phi_2 = 2(x),2(-x)$; $\phi_3 = 8(x),8(-x)$; $\phi_4 = x$; $\phi_5 = x,-x$; $\phi_6 = -x$; and receiver $= x,-x$. Quadrature detection in the ^{1}H dimension (t_1) is achieved by simultaneous incrementation of ϕ_3 and ϕ_4. All other parameters are as marked in the legend to Figure 3B.

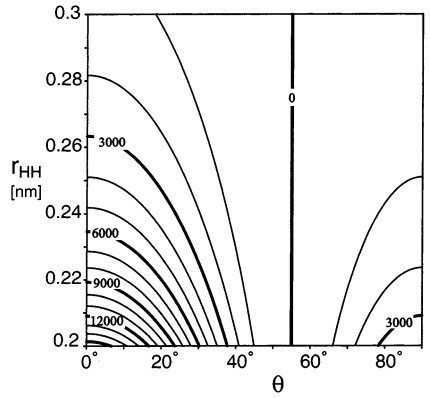

Figure 5. Contour plot representation of the geometrical factor ($P_2(\cos\theta)/r_{HH}^3)^2$ versus the distance r_{HH} (nm) and the angle θ in degree. In the plot region shown, the geometrical factor ranges from 0 to 15 625 nm^{-6}.

into $2H_z^1H_y^2$. Between time points *c* and *d*, the same Γ_1 cross-correlation process transforms $2H_y^1H_z^2$ back into $2H_y^1C_z^1$. The subsequent part of the pulse scheme is the same as that following time point *b* in Figure 3B, and introduces ^{13}C modulation in the t_2 dimension. The out-and-back RACT therefore results in a cross-peak at ($\omega_{H2},\omega_{C1},\omega_{H1}$) for magnetization originating on proton H^1, with an intensity described by

$$I_T = I_0 \sinh(-\Gamma_1\Delta_1)\sinh(-\Gamma_1\Delta_2)\exp[-R_2(\Delta_1+\Delta_2)] \quad (9)$$

Of course, magnetization originating on H^2 gives rise to a similar cross-peak, but with its intensity governed by $\sinh(-\Gamma_2\Delta_1)\sinh(-\Gamma_2\Delta_2)$. To determine the quantitative magnitude of this cross-correlation term, a reference experiment is designed of the same total duration, but with essentially complete $H^1 \rightarrow C^1 \rightarrow H^1$ magnetization transfer accomplished through J_{CH} de- and rephasing (Figure 4), yielding an intensity I_{Ref}. As $\Gamma\Delta \ll 1$, the ratios of the two intensities may be written as

$$\frac{I_T}{I_{Ref}} = \sinh(-\Gamma_{CH,HH}^{DD,DD}\Delta_1)\sinh(-\Gamma_{CH,HH}^{DD,DD}\Delta_2)$$
$$\approx \frac{4\Delta_1\Delta_2}{25}\left(\frac{\mu_o}{4\pi}\hbar\gamma_H^2\,\xi_{CH}^{DD}\tau_C\right)^2\left(\frac{P_2(\cos\theta)}{\langle r_{HH}^3\rangle}\right)^2 \quad (10)$$

The theoretical dependence of the I_T/I_{Ref} ratio on the geometry is presented in Figure 5. For a local geometry close to regular antiparallel β-sheets ($r_{HH} = 2.4$ Å, $\theta = 25°$), the experimental

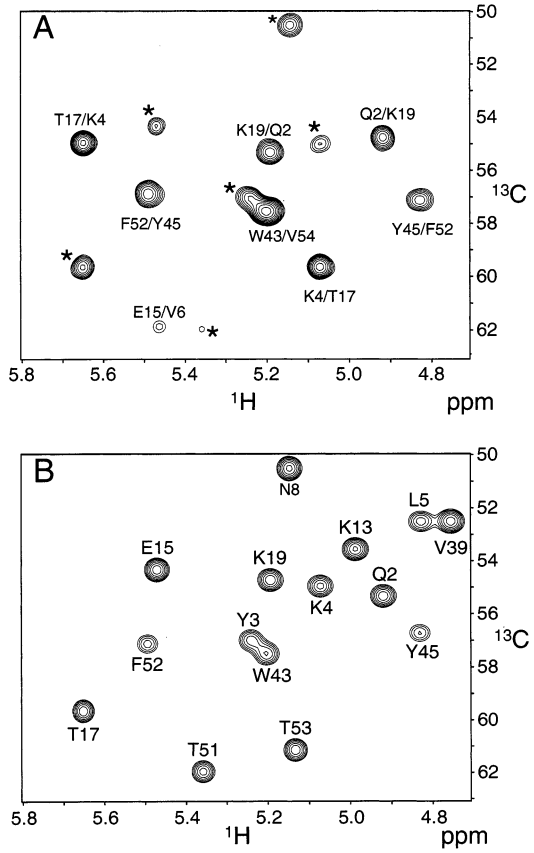

Figure 6. Small sections of 2D ^{1}H−^{13}C correlation spectra of protein GB3. (A) Unidirectional RACT spectrum, recorded with the scheme of Figure 3A, using the room-temperature probe and a total experiment time of 12 h. The data matrix consisted of $96(t_1) \times 1024(t_2)$ data points, with acquisition times of 10.6 (t_1) and 68 ms (t_2). RACT delays: $\Delta_1 = 20.93$ ms; $\Delta_2 = 24.41$ ms. Interresidue RACT correlations are labeled with the corresponding residue numbers; residual diagonal peaks are marked with asterisks. Correlations between residues 54 and 43 and between 6 and 15 fall outside the regions shown but are presented in the Supporting Information. (B) Same spectral region in the regular ^{1}H−^{13}C HSQC spectrum.

ratio will be very sensitive to small variations of the conformation: an independent modification of the angle by 4° or of the interproton distance by 0.1 Å results in a variation of the I_T/I_{Ref} ratio by more than 25%.

Equation 10 applies to the integrated intensities of the reference peaks and cross-peaks. However, for maximum t_1 durations that are shorter than the difference in the inverse relaxation rates of $2H_y^2H_z^1$ and H_y^1, the difference in cross-peak and reference line shapes is negligible, and peak heights may be used instead.

Application to Protein G. The feasibility of magnetization transfer via dipole−dipole cross-correlated relaxation in proteins is demonstrated for two systems: GB3 and HIV protease. We first discuss application to GB3, a domain for which a 1.1-Å X-ray structure is available.[46] This atomic resolution structure also allows for quantitative validation of eq 10. GB3 contains two sets of antiparallel β-strands. A region of the 2D RACT correlation spectrum, recorded with the pulse sequence of Figure 3A, is shown in Figure 6A. It shows eight cross-peaks, corresponding to five different H_α pairs (the two remaining cross-peaks fall outside of the region shown). As expected, they all involve correlations between proximate H_α nuclei on

(46) Derrick, J. P.; Wigley, D. B. *J. Mol. Biol.* **1994**, *243*, 906−918.

antiparallel-paired β-strands. For reference, the corresponding HSQC spectral region is shown in Figure 6B. Correlations marked by asterisks in Figure 6A correspond to direct, one-bond correlations which are incompletely suppressed as a result of the heterogeneity of $^1J_{CH}$ values, which range from 135 to 153 Hz in this domain (B. Ramirez, personal communication). To minimize these residual signals for β-sheet residues, Δ_1 and Δ_2 were optimized for $^1J_{CH} = 143.4$ Hz, which corresponds to the middle of the range of values expected in β-strands.[47] These residual peaks are particularly strong for small proteins such as GB3, for which the optimal Δ_1 and Δ_2 durations are rather long (ca. 20−25 ms at 15 °C). For larger proteins, such one-bond correlations are much less intense, owing to the shorter optimal transfer delays (Figure 1). Nevertheless, they frequently remain observable for α-helical residues, which typically have larger $^1J_{CH}$ values.

One-bond and RACT correlations can easily be distinguished by the 3D version of the RACT experiment (Figure 3B). For example, consider the correlation between residues 43 and 54 of protein GB3 in Figure 6A. Because the chemical shifts of the two $^{13}C_\alpha$ nuclei are very similar, it is unclear if the correlation observed in spectrum 6A corresponds to a residual diagonal peak, caused by *J*-mismatching, or a real cross-peak due to RACT. Analysis of the 3D spectrum shows a well-resolved peak at (ω_{H54},ω_{C43},ω_{H43}) frequencies (Supporting Information), confirming that the peak results from cross-correlation.

Correlation with Structure. Inspection of the β-sheet topology of GB3 suggests that there are six pairs of H_α nuclei for which RACT correlations are expected. However, no correlations are observed for the pair involving residues 8 and 13; all others are observed (Figure 6A and Supporting Information Figure 1). A more quantitative analysis of the 3D structure of GB3 (PDB code 2IGD) reveals a noncanonical geometry for the 8−13 pair. The angle between vectors $C_\alpha^8-H_\alpha^8$ and $H_\alpha^8-H_\alpha^{13}$ (θ_1 in Figure 2 when substituting $C_\alpha^1 = C_\alpha^8$, $H_\alpha^1 = H_\alpha^8$, and $H_\alpha^2 = H_\alpha^{13}$) equals 53°, which is very close to the condition where the angular part of eq 3 equals zero (magic angle). This therefore precludes the observation of unidirectional transfer between residues 8 and 13 (cf. eqs 7 and 8). In contrast, in spectra recorded with the out-and-back transfer scheme (Figure 4), an additional correlation at frequencies (ω_{H8},ω_{C13},ω_{H13}) is observed (data not shown). In this out-and-back experiment, the observed intensity does not depend on the $C_\alpha^8-H_\alpha^8-H_\alpha^{13}$ angle, which is responsible for the near-zero intensity in the unidirectional experiment.

The good qualitative agreement between the observed cross-peaks and the GB3 structure suggests that cross-correlated relaxation rates can yield quantitative information for structure determination. However, the structural dependence of eq 10 applies for an isolated three-spin system. In a protein, the presence of other spins complicates the situation. In particular, the $^1H-^1H$ dipolar interactions with additional neighboring protons in the protein need to be considered. The cross-correlated relaxation rate itself, $\Gamma^{DD,DD}_{C1H1,H1H2}$, remains unaffected by the presence of additional ^1H spins. For the autorelaxation rates, to a very good approximation, only the $^1H-^1H$ dipolar interactions need to be considered. Dipolar interactions between H^1 and additional neighboring spins affect the autocorrelated relaxation rate $R(H^1_+)$, $R(2H^1_+C^1_z)$, $R(2H^1_+H^2_z)$, and $R(4H^1_+H^2_zC^1_z)$ equally, and therefore to first order do not affect the intensity ratio of eq 10. Dipolar interactions between H^2 and neighboring protons affect only the $R(2H^1_+H^2_z)$ and $R(4H^1_+H^2_zC^1_z)$ rates. Increases in these latter relaxation rates correspond to the H^2 longitudinal relaxation induced by additional neighboring protons. In the slow tumbling limit, and neglecting internal motion, the increase in effective relaxation rates falls in the 3−9% range if the additional neighboring protons are approximated by a single "pseudo-proton" placed at a distance, $r = [\sum_i (r_i)^{-6}]^{-1/6}$, in the 2.3−1.9 Å range from H^2.

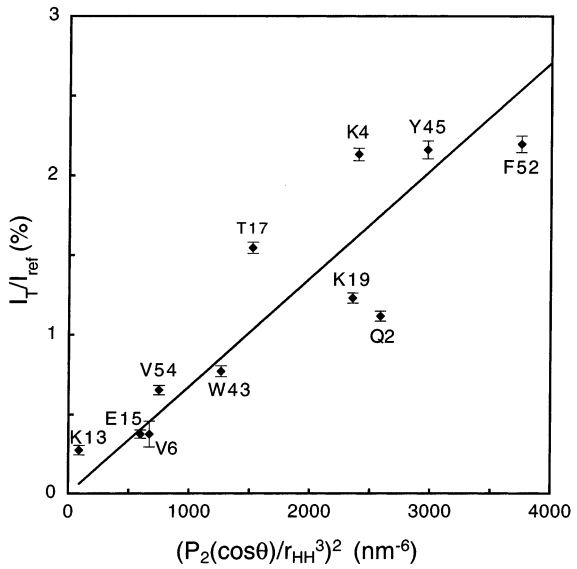

Figure 7. Correlation between the observed ratio I_T/I_{Ref} and the geometrical factor, calculated from the 1.1 Å X-ray structure of protein GB3, refined with anisotropic *B* factors (PDB code 2IGD),[46] to which protons were added with X-PLOR using idealized covalent geometry.[61] Labeling of the data points corresponds to the residue for which H_α is observed during t_3. Pearson's correlation coefficient, R_P, equals 0.89, and the pairwise rmsd equals 504 nm^{-6}. Data were acquired at 6.5 °C with the pulse scheme of Figure 4. RACT and reference spectra were recorded in 19 and 5 h, respectively, on a 600-MHz NMR spectrometer equipped with a cryogenic probehead. Prior to zero-filling, the raw data matrix consisted of $14(t_1) \times 48(t_2) \times 1024(t_3)$ data points, with acquisition times of 7.8 (t_1), 5.3 (t_2), and 57 ms (t_3). RACT delays: $\Delta_1 = 10.46$ ms; $\Delta_2 = 13.95$ ms. The best-fit line corresponds to a rotational diffusion correlation time of 6.3 ns (when accounting for internal motion by scaling all relaxation rates by $S^2 = 0.8$, and accounting for the effect of remote protons by a uniform 0.97 scaling factor). The corresponding dipole−dipole cross-correlated rates range from 4.4 (Lys[13]) to 12.5 Hz (Phe[52]).

The implication of the violation of the secular approximation in eq 2 when applied to a protein was determined using eq 40 of ref 33, extended to take into account neighboring protons. For the GB3 data, the I_T/I_{Ref} ratio (eq 10) decreases by a factor 0.97 ± 0.01 when again accounting for the additional protons by a single "pseudo-proton" placed at a distance of 2.1 ± 0.2 Å from H^α. This 3% systematic underestimate in the I_T/I_{Ref} ratio is comparable to the measurement error and therefore may be safely ignored.

Figure 7 plots the I_T/I_{Ref} ratio measured for the 11 H_α protons in GB3 as a function of the geometric factor $(P_2(\cos\theta)/r_{HH}^3)^2$, calculated from its 1.1-Å resolution X-ray structure. The slope of the solid line in this figure corresponds to a τ_c value of 6.3 ns, which is within 10% from previous NMR relaxation results,[48−50] corrected for differences in temperature and solvent viscosity (D_2O vs H_2O).[51] Considering the extremely steep

(47) Vuister, G. W.; Delaglio, F.; Bax, A. *J. Biomol. NMR* **1993**, *3*, 67−80.

dependence of the ratio on local geometry, with a Pearson's correlation coefficient $R_P = 0.89$, the observed correlation is remarkably good. The largest outlier in Figure 7 is observed for Gln^2-H_α, but this residue differs by a T2Q substitution from the amino acid sequence used for the X-ray crystallographic study.[46] The root-mean-square (rms) deviation between experimental and predicted data is 504 nm^{-6}. Assuming an average β-sheet geometry ($r_{H1H2} = 2.4$ Å and $\theta_1 = 25°$; see Figure 2 for notation), this deviation corresponds either to a variation of 0.07 Å for the interproton distance or to a 3.5° change in θ, which is comparable to the errors in these distances and angles on the basis of the atomic coordinate uncertainties in the 1.1-Å X-ray structure. For comparison, even with the most careful analysis of NOE data using relaxation-matrix-based refinement, distance restraints generally carry an uncertainty of at least 0.2 Å.[52]

Comparison of the geometric factor $(P_2(\cos\theta)/r_{HH}^3)^2$ for GB3 (PDB code 2IGD)[46] and the highly homologous crystal structure of the first Igg-binding domain of protein G (PDB code 1PBG)[53] shows a lower correlation ($R_P = 0.64$) than comparison of our experimental, NMR-derived geometric factors to 1PBG ($R_P = 0.77$). It is also interesting to note that correlation of the NMR-derived geometric factors with the 1.1-Å crystal structure of GB3, refined with isotropic *B*-factors (PDB code 1IGD),[46] yields a lower R_P (0.79) than the correlation with the GB3 X-ray structure refined with anisotropic *B*-factors ($R_P = 0.89$). These results therefore underscore the high precision of the structural restraints that can be extracted from the cross-correlation data.

Application to a 22-kDa Protein. As discussed in Theoretical Basis section, one important feature of RACT transfer is that its efficiency does not decrease with increasing size of the molecule (Figure 1). Therefore, the RACT experiment is well suited for the study of larger β-sheet-rich proteins too, provided that high-quality $^1H-^{13}C$ one-bond correlation spectra are obtainable. To demonstrate the utility for larger proteins, 3D unidirectional and out-and-back spectra have been recorded for a sample of the 22-kDa homodimeric HIV-1 protease, complexed with inhibitor DMP323.[54]

Examples of unidirectional correlations observed in the HIV-1 protease are shown for the H_α protons of residues Gly^{48}, Glu^{65}, and Ile^{72} (Figure 8). On average, the same correlations in the out-and-back version of the experiment are about 15% weaker, owing to signal decay during the additional (non-constant-time) ^1H evolution period (Supporting Information Figure 2). Despite the low concentration of this sample (0.4 mM), the spectrum shows a total of 23 correlations involving H_α protons, with a signal-to-noise ratio ranging from 5 to 26. All the observed correlations correspond to 12 distinct pairs of H_α protons on adjacent β-strands (Figure 8B). Comparison with the secondary structure of the protein[55] shows that only pairs $Ile^{13}-Ile^{66}$, $Ile^{15}-Ile^{64}$, and $Thr^{31}-Ile^{85}$ do not give rise to any observable correlations. A more detailed analysis of different crystal structures (PDB codes 1MET and 1MES) reveals noncanonical structure for the two last pairs, with interproton distances larger than 3 Å, which correspond to RACT rates that are too low to observe such transfers. From the remaining 13 pairs, one involves an intermonomer contact between the H_α protons of Leu^{97}, yielding only a single correlation. From the remaining

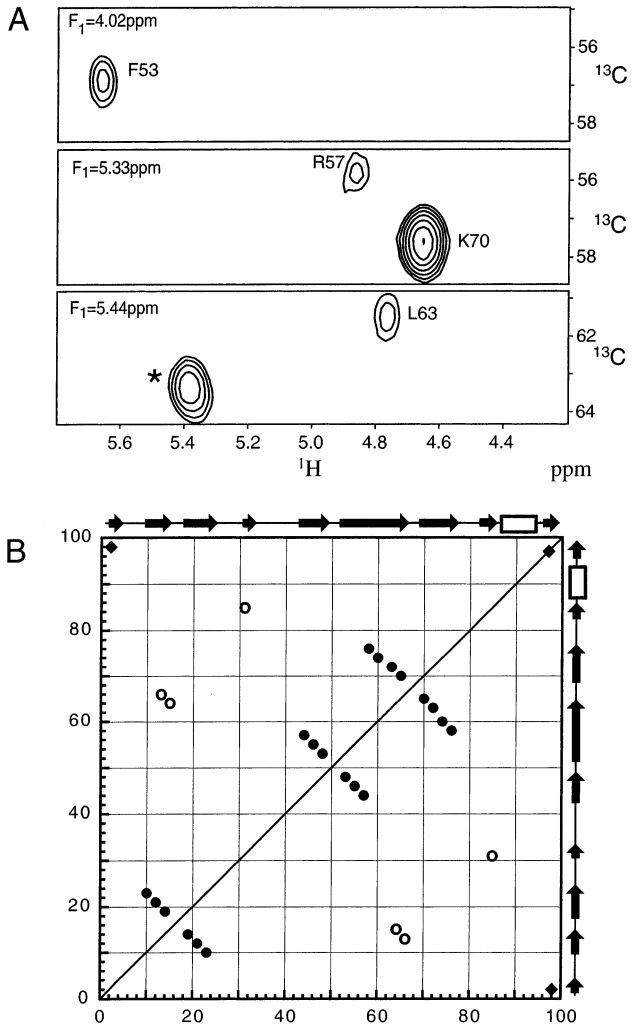

Figure 8. (A) Selected (F_2,F_3) sections taken from the unidirectional 3D RACT spectrum at F_1 frequencies marked in the figure and recorded with the pulse scheme of Figure 3B on HIV-1 protease for a total measuring time of 35 h. Sections shown are taken at F_1 frequencies of H_α of residues Gly^{48}, Glu^{65}, and Ile^{72}. A residual one-bond correlation for Pro^{44} (which has a large $^1J_{H\alpha C\alpha} = 151$ Hz; $H_\alpha = 5.38$ ppm) is marked by an asterisk; the shoulder of its correlation to Arg^{57}-H_α is visible in the center panel. The time domain data matrix consisted of $32(t_1) \times 48(t_2) \times 512(t_3)$ data points, with acquisition times of 7.8 (t_1), 5.3 (t_2), and 32 ms (t_3). RACT delays: $\Delta_1 = 10.46$ ms; $\Delta_2 = 13.95$ ms. To increase the t_1 resolution, the first H_α REBURP pulse was shortened to 1.8 ms. Cross-peaks due to RACT are labeled with the residue number for which H_α was detected during t_3. (B) Topology of HIV-1 protease, with observed RACT correlations marked by solid circles. Correlations expected from secondary structure but with indetectably small RACT rates are marked by open circles. The interchain correlations between H_α protons of pair Gln^2/Asn^{98} and the two H_α protons of the two Leu^{97} residues (on the diagonal) are marked by solid diamonds.

(48) Barchi, J. J.; Grasberger, B.; Gronenborn, A. M.; Clore, G. M. *Protein Sci.* **1994**, *3*, 15−21.
(49) Tillett, M. L.; Blackledge, M. J.; Derrick, J. P.; Lian, L. Y.; Norwood, T. J. *Protein Sci.* **2000**, *9*, 1210−1216.
(50) Seewald, M. J.; Pichumani, K.; Stowell, C.; Tibbals, B. V.; Regan, L.; Stone, M. J. *Protein Sci.* **2000**, *9*, 1177−1193.
(51) Cho, C. H.; Urquidi, J.; Singh, S.; Robinson, G. W. *J. Phys. Chem. B* **1999**, *103*, 1991−1994.
(52) Thomas, P. D.; Basus, V. J.; James, T. L. *Proc. Natl. Acad. Sci. U.S.A.* **1991**, *88*, 1237−1241.
(53) Gallagher, T.; Alexander, P.; Bryan, P.; Gilliland, G. L. *Biochemistry* **1994**, *33*, 4721−4729.
(54) Lam, P. Y. S.; Jadhav, P. K.; Eyermann, C. J.; Hodge, C. N.; Ru, Y.; Bacheler, L. T.; Meek, J. L.; Otto, M. J.; Rayner, M. M.; Wong, Y. N.; Chang, C. H.; Weber, P. C.; Jackson, D. A.; Sharpe, T. R.; Ericksonviitanen, S. *Science* **1994**, *263*, 380−384.
(55) Wlodawer, A.; Erickson, J. W. *Annu. Rev. Biochem.* **1993**, *62*, 543−585.

25 expected cross-peaks, only the correlations between H_α protons of Ile^{13} and Ile^{66} are not observed. This interaction involves an unfavorable angle between vectors $C_\alpha^{13}-H_\alpha^{13}$ and $H_\alpha^{13}-H_\alpha^{66}$ ($\theta = 41°$, making the corresponding cross-correlated relaxation rate the smallest predicted one).

Quantitative comparison of I_T/I_{Ref} ratios with the HIV protease structure is limited by the resolution of the available X-ray structures. Two structures of highly homologous HIV-1 proteases in complex with the DMP323 inhibitor have been solved by X-ray crystallography at a resolution of 1.9 Å.[56] The two crystal structures differ from the NMR sample used by six-point mutations (residues 7, 33, 63, 67, 95, 84 for PDB entry 1MES, and 7, 33, 63, 67, 95, 82 for PDB entry 1MET), and by two-point mutations from one another. Despite the fact that the structures have very similar backbone coordinates, with pairwise backbone rmsd's of less than 0.2 Å over the secondary structure regions of the protein, comparison of the relevant interproton distances and angles between the two structures results in a standard deviation of 0.13 Å and 5.8°. As expected, therefore, a poor correlation ($R_P = 0.46$) is obtained when comparing the geometrical factors, $[P_2(\cos\theta)/r_{HH}^3]^2$, for the two 1.9-Å resolution X-ray structures (Supporting Information Figure 3).

When structural differences are small, the averages of the corresponding geometric factors are very similar to the geometrical factors of the average structure. This averaging procedure therefore reduces the effect of small, largely random coordinate errors in the X-ray structures. As a result, a slightly better degree of correlation ($R_P = 0.62$) is obtained when comparing the experimentally measured geometrical factors with the average of the geometric factors for the two crystal structures (Supporting Information Figure 4). However, considering that the scatter between the geometrical factors derived from the different crystal structures is even larger, it is likely that the spread in the correlation between the NMR data and the averaged X-ray derived geometric factors remains dominated by the uncertainty in the X-ray coordinates. This indicates that it will be beneficial to use the experimental RACT rates as additional parameters in structure calculation and refinement.

Conclusions

Our study demonstrates that magnetization transfer between uncoupled nuclei by means of dipole−dipole cross-correlated relaxation is feasible in proteins. In the slow tumbling limit, the efficiency of such transfer is insensitive to the rotational correlation time, and therefore the RACT experiments are particularly promising for the study of larger proteins. In β-sheets, RACT between H_α protons on adjacent strands is exquisitely sensitive to the local geometric parameters. This suggests that RACT rates will be particularly useful for refining the local structure of β-sheets in proteins.

Quantitative measurement of RACT rates is relatively straightforward. A wide range of different types of interactions in proteins and nucleic acids, involving atoms in separate, noncovalently linked segments, can be envisioned to yield structurally meaningful information. Structure refinement to improve agreement with the experimental RACT rates simultaneously involves angular and distance terms and is relatively similar to refinement of protein structures against $^1H-^1H$ dipolar couplings.[57] Together with the use of dipolar couplings, RACT rates are expected to make it possible to determine the structure of biological macromolecules with unprecedented accuracy.

Acknowledgment. We thank J.-P. Simorre and B. Brutscher for stimulating discussions, B. Ramirez and J. Louis for the preparation of $^{13}C/^{15}N$-labeled protein samples, and D. A. Torchia and R. Ishima for providing assignments of HIV-1 protease. This work was supported by fellowship of Human Frontier Science Program and the AIDS Targeted Anti-viral Program of the Office of the Director of the National Institutes of Health.

Supporting Information Available: Four figures showing (1) selected regions from the unidirectional 3D RACT spectrum of GB3, (2) selected regions from the "out-and-back" 3D RACT spectrum of HIV-1 protease, (3) correlation of the geometrical factors for opposing $C_\alpha H_\alpha$ pairs in antiparallel β-sheets in HIV protease, derived from two crystal structures, and (4) plot of experimental I_T/I_{Ref} ratio against the averaged geometrical factors in antiparallel β-sheets in HIV protease, derived from two crystal structures (PDF). This material is available free of charge via the Internet at http://pubs.acs.org.

JA020511G

(56) Ala, P. J.; Huston, E. E.; Klabe, R. M.; McCabe, D. D.; Duke, J. L.; Rizzo, C. J.; Korant, B. D.; DeLoskey, R. J.; Lam, P. Y. S.; Hodge, C. N.; Chang, C. H. *Biochemistry* **1997**, *36*, 1573−1580.
(57) Tjandra, N.; Marquardt, J.; Clore, G. M. *J. Magn. Reson.* **2000**, *142*, 393−396.
(58) Geen, H.; Freeman, R. *J. Magn. Reson.* **1991**, *93*, 93−141.
(59) Shaka, A. J.; Barker, P. B.; Freeman, R. *J. Magn. Reson.* **1985**, *64*, 547−552.
(60) Wu, Z. R.; Tjandra, N.; Bax, A. *J. Biomol. NMR* **2001**, *19*, 367−370.
(61) Brunger, A. T. *XPLOR: A System for X-ray Crystallography and NMR*, version 3.1; Yale University Press: New Haven, 1993.